Cell Reports

Meta-analysis of Chromatin Programming by Steroid Receptors

Graphical Abstract

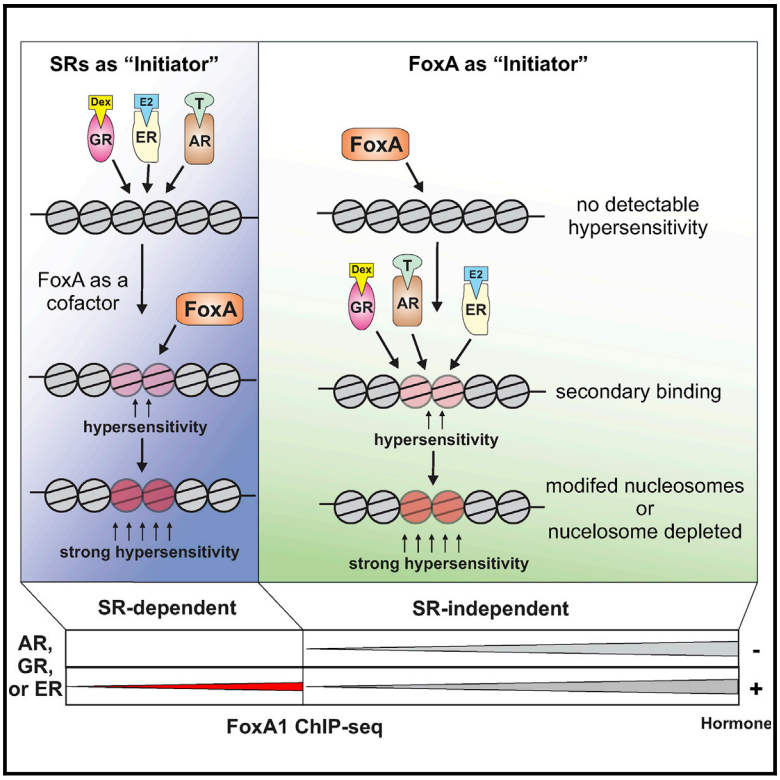

Highlights

- Chromatin binding of pioneer factor FOXA1 can be modulated by a steroid hormone
- Reprogramming of FOXA1 binding is evident in breast and prostate cancer cells
- This modulation is shown from datasets representing seven independent investigators

Authors

Ville Paakinaho, Erin E. Swinstead, Diego M. Presman, Lars Grøntved, Gordon L. Hager

Correspondence

hagerg@dce41.nci.nih.gov

In Brief

It is widely accepted that only pioneer transcription factors such as FOXA1 can reprogram chromatin for secondary transcription factor binding. Paakinaho et al. report through meta-analysis of published independent ChIP-seq datasets from several laboratories that the chromatin binding of FOXA1 can be reprogrammed by steroid hormone treatment.

Paakinaho et al., 2019, Cell Reports *28*, 3523–3534
September 24, 2019
https://doi.org/10.1016/j.celrep.2019.08.039

CellPress

Cell Reports
Matters Arising

Meta-analysis of Chromatin Programming by Steroid Receptors

Ville Paakinaho,[1] Erin E. Swinstead,[2] Diego M. Presman,[3] Lars Grøntved,[4] and Gordon L. Hager[2,5,*]
[1]Institute of Biomedicine, University of Eastern Finland, Kuopio, 70211 Kuopio, Finland
[2]Laboratory of Receptor Biology and Gene Expression, National Cancer Institute, NIH, Bethesda, MD 20892-5055, USA
[3]Instituto de Fisiología, Biología Molecular y Neurociencias (IFIBYNE-UBA-CONICET), Universidad de Buenos Aires, Facultad de Ciencias Exactas y Naturales, Buenos Aires C1428EGA, Argentina
[4]Department of Biochemistry and Molecular Biology, University of Southern Denmark, 5230 Odense M, Denmark
[5]Lead Contact
*Correspondence: hagerg@dce41.nci.nih.gov
https://doi.org/10.1016/j.celrep.2019.08.039

SUMMARY

Transcription factors (TFs) must access chromatin to bind to their response elements and regulate gene expression. A widely accepted model proposes that only a special subset of TFs, pioneer factors, can associate with condensed chromatin and initiate chromatin opening. We previously reported that steroid receptors (SRs), not considered pioneer factors, can assist the binding of an archetypal pioneer, the forkhead box protein 1 (FOXA1), at a subset of receptor-activated enhancers. These findings have been challenged recently, with the suggestion that newly acquired data fully support the prevailing pioneer model. Here, we reexamine our results and confirm the original conclusions. We also analyze and discuss a number of available datasets relevant to chromatin penetration by SRs and find a general consensus supporting our original observations. Hence, we propose that chromatin opening at some sites can be initiated by SRs, with a parallel recruitment of factors often treated as having a unique pioneer function. This Matters Arising paper is in response to Glont et al. (2019), published in *Cell Reports*.

INTRODUCTION

How transcription factors (TFs) penetrate chromatin and break the nucleosome barrier to access their specific response elements is central to an understanding of transcriptional regulation. A widely followed paradigm argues that a special class of proteins, pioneer factors, have the unique ability to access nucleosome embedded DNA. These factors facilitate chromatin remodeling and allow the binding of secondary TFs, which otherwise would not be able to access their target DNA sequence (Zaret and Carroll, 2011). This select group of pioneer proteins includes reprograming factors such as OCT4, SOX2, and KLF4 and lineage-specifying TFs such as GATA binding protein (GATA) and forkhead box protein (FOXA) family members, PU.1, and C/EBPα, among others (Mayran and Drouin, 2018).

Multiple mechanisms have been proposed for the penetration of closed chromatin by pioneer factors. The forkhead box protein 1 (FOXA1) can bind and induce nucleosome rearrangements via its winged-helix domain, similar to the H1 linker histone, by an adenosine triphosphate (ATP)-independent mechanism (Cirillo et al., 2002, 1998). However, this mechanism cannot be universal, as many pioneer factors lack the winged-helix domain. In addition, ATP-dependent chromatin remodelers have been linked to GATA3 and OCT4 actions (King and Klose, 2017; Takaku et al., 2016), suggesting ATP plays an important role in pioneer activity. Moreover, pioneer factors have some limitations in their ability to access chromatin, as ectopic expression of FOXA2 and GATA4 still exhibits cell-type specific binding (Donaghey et al., 2018). The latter suggests the chromatin landscape, in addition to intrinsic properties of a given TF, is a major determinant to access enhancer elements.

Steroid receptors (SRs) are ligand-regulated TFs involved in several key physiological processes (Chen, 2008). Under the pioneer paradigm, these receptors are classified as secondary factors (Zaret and Carroll, 2011). However, several lines of evidence disagree with this model. For example, the glucocorticoid receptor (GR) shows bona fide pioneer properties, as it can access nucleosomal enhancers (Archer et al., 1991; Richard-Foy and Hager, 1987) and open chromatin by recruiting the chromatin remodeler BRG1 (Hoffman et al., 2018; Johnson et al., 2018). Moreover, a "super receptor" version of the GR (GR-P481R) transcends tissue specificity by accessing (and opening) enhancer sites that wild-type receptors can only access in other tissues (Paakinaho et al., 2019).

The ability to assist secondary TFs' access to chromatin does not appear to be a defining or exclusive characteristic of pioneer factors, as the GR and the estrogen receptor (ER) can assist each other to bind enhancers by a mechanism called dynamic-assisted loading (Miranda et al., 2013; Voss et al., 2011). Also, activation of the GR can facilitate recruitment of AP1 and C/EBPβ to chromatin (Grøntved et al., 2013; He et al., 2013). Taken together, SRs present "pioneer-like" properties in a chromatin context-dependent manner, effectively blurring the hitherto defined line between pioneer and non-pioneer factors. In fact, a binary classification may not be sufficient to capture the complexity and diversity of the interaction between TFs and chromatin, as at least five types of interactions between TFs

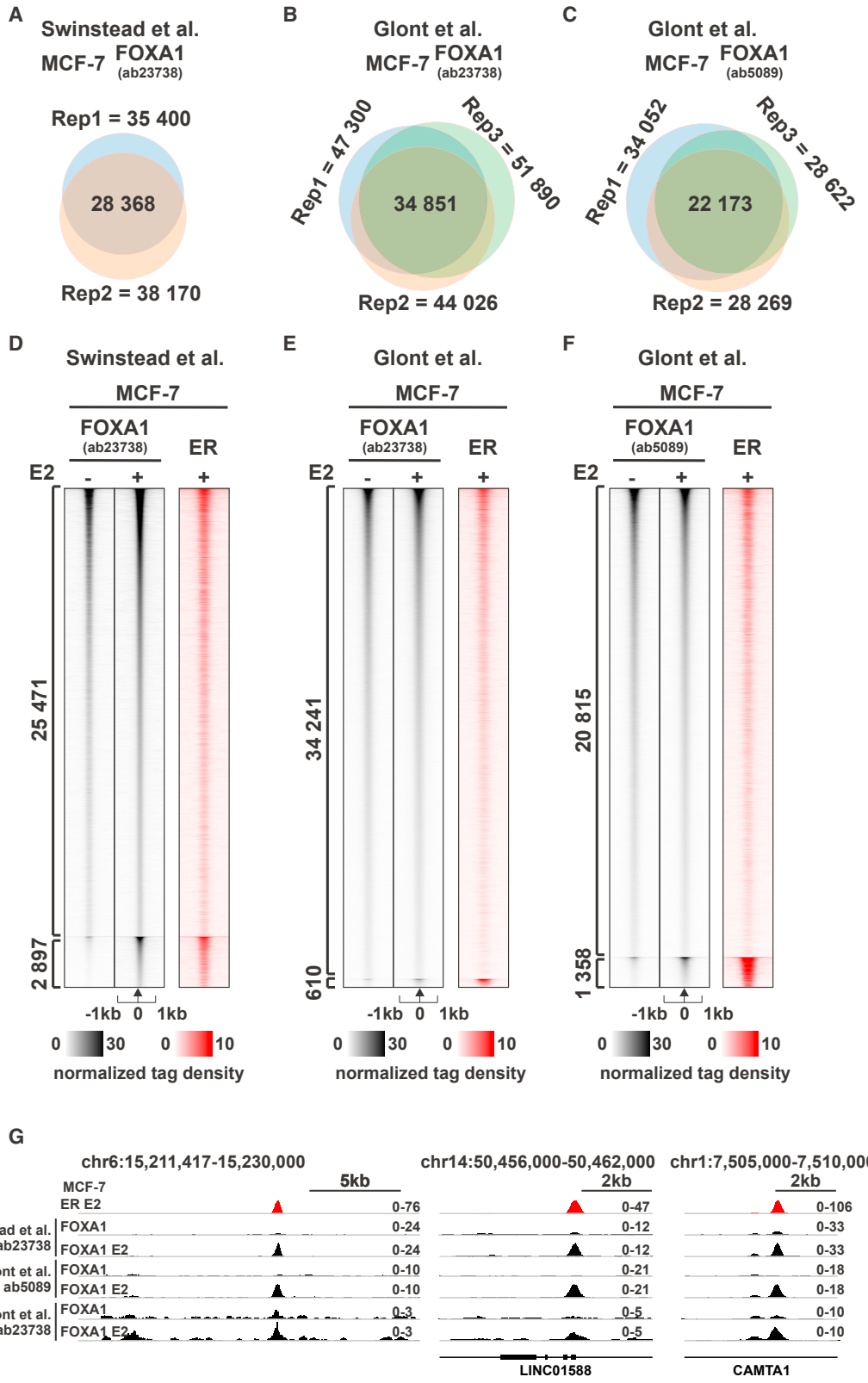

(legend on next page)

and the nucleosome have been recently described *in vitro* (Zhu et al., 2018).

In 2016, we reported that ERs and GRs can induce the binding of the pioneer factor FOXA1 to chromatin through dynamic transitions of chromatin accessibility (Swinstead et al., 2016). This result challenged the prevailing pioneer factor model, as elaborated on by Carroll and colleagues (Hurtado et al., 2011; Zaret and Carroll, 2011), arguing that FOXA1 is an obligate factor needed for an ER's interaction with chromatin. Two subsequent reports have questioned the quality and interpretation of the original datasets contradicting the canonical FOXA1 pioneer model (Glont et al., 2019; Zaret et al., 2016). Here, we re-analyze our original data (Swinstead et al., 2016), compare the newly acquired results with the opposing findings (Glont et al., 2019), and subsequently reconfirm our original conclusions. Moreover, we have analyzed several publicly available datasets relevant to chromatin penetration by SRs (Franco et al., 2015; Hurtado et al., 2011; Kong et al., 2011; Liu et al., 2014; Malinen et al., 2017; Pihlajamaa et al., 2014; Toropainen et al., 2015). All of these studies show that a considerable subset of FOXA1 binding depends on the activation of a SR, in agreement with our original publication.

RESULTS

Activation of the ER Induces the Binding of FOXA1 in MCF-7 and ZR-75-1 Cells

To carefully address the concerns raised by Glont et al. (2019), using the same criteria for peak identification, tag quantification, and data visualization, we re-analyzed the recent FOXA1 ChIP-seq datasets generated by Carroll and colleagues together with our original FOXA1 ChIP-seq datasets (Swinstead et al., 2016). One critique Glont et al. (2019) highlighted was an inconsistency between replicates of our original data. Indeed, the variability between replicates did not allow subsequent statistical analysis by approaches such as EdgeR and DESeq2 (Love et al., 2014; Robinson et al., 2010). To account for this, we called replicate concordant peaks. In contrast to this approach, Glont et al. (2019) did not call ChIP-seq peaks from each individual replicate samples, but instead called peaks after combining all replicates together. We reperformed FOXA1 peak identification from each individual biological replicate sample (Figures 1A–1C and S1B–S1D) from both studies. This shows a similar overlap of called peaks between replicates of our original sets (Swinstead et al., 2016) and most of Glont et al. (2019) datasets. One ZR-75-1 FOXA1 replicate (ab5089) from Glont et al. showed more than 50% fewer called peaks compared to the other replicates (Figure S1D). Furthermore, our peak calling and replicate concordant analysis was much more stringent than that used by Carroll and colleagues (Glont et al. (2019), as we called roughly 50% fewer FOXA1 ChIP-seq peaks with each antibody in both the MCF-7 and ZR-75-1 cell lines. This highlights that the less stringent peak calling used by Glont et al. can potentially lead to an overestimation of FOXA1 peaks and an underrepresentation of ligand-induced FOXA1 binding.

Subsequently, we determined whether activation of the ER by 17β-estradiol (E2) can induce the chromatin binding of FOXA1, as we indicated in our original work (Swinstead et al., 2016) (see STAR Methods for details). All FOXA1 ChIP-seq datasets show E2-induced FOXA1 binding sites (Figures 1D–1F and S1E–S1G), including separate biological replicate samples (Figures S1A and S1H). Our data showed 2,897 E2-induced FOXA1 (with ab23738) sites in MCF-7 cells (Figure 1D), while Glont et al. (2019) showed 610 sites with ab23738 (Figure 1E) and 1,358 sites with ab5089 (Figure 1F). We found a similar trend but lower numbers of E2-induced FOXA1 sites in the ZR-75-1 cells (Figures S1E–S1G). As expected, ER binding was prevalent at the E2-induced FOXA1 binding sites, suggesting an active role of the ER in reprogramming chromatin for FOXA1 binding. This is further highlighted in representative genome browser tracks (Figures 1G and S1I). Thus, we identify hormone-induced FOXA1 binding in MCF-7 cells and ZR-75-1 cells using two independent datasets, and the original conclusions are valid. It is of value to note that the variability between the independent datasets likely reflects slight differences in the clonal cell lines (Ben-David et al., 2018), culture conditions, and ChIP protocols.

Motifs for Both the ER and FOXA1 Are Enriched at E2-Induced FOXA1 Sites

A major conclusion by Glont et al. (2019) was that the E2-induced FOXA1 sites are generated by "shadow" binding events due to chromatin looping of FOXA1. Carroll and colleagues based this conclusion on the lack of forkhead motifs at the E2-induced FOXA1 sites. However, no details from the motif analyses were provided, and only one enriched motif was indicated. We performed extensive motif analyses of the E2-induced FOXA1 sites (see STAR Methods for details). A *de novo* motif analysis indicates a strong enrichment of both the estrogen response element (ERE) and the forkhead motifs at E2-induced FOXA1 sites in all datasets, and in both MCF-7 and ZR-75-1 cells (Figures 2A and S2A). To assess the motif enrichment data in more detail, we compared the motif scores of the ERE and FOXA1

Figure 1. E2-Induced Binding of FOXA1 in MCF-7 Cells

(A–C) Comparison of identified FOXA1+E2 peaks from biological replicate samples using datasets from Swinstead et al. (2016) (A) and Glont et al. (2019) (B and C). Numbers of peaks identified in each replicate and the concordant peaks are shown. Used FOXA1 antibody is depicted in the parentheses.

(D–F) Heatmaps represent FOXA1 (black) ChIP-seq data from Swinstead et al. (2016) (D) and Glont et al. (2019) (E and F) with unchanged sites on top of the heatmap and E2-induced FOXA1 sites on the bottom of the heatmap. Heatmaps of ER (red) represent ChIP-seq data from Swinstead et al. (2016).The number of binding sites is shown on the left of the heatmap. Each heatmap represents ±1 kb around the center of the FOXA1 peak. Binding intensity scale is noted below on a linear scale. Heatmaps are sorted based on FOXA1+E2 binding intensity. All heatmaps are normalized to a total of 10 million reads and to tags per bp per site. Used FOXA1 antibody is depicted in the parentheses.

(G) Three representative genome browser track examples of E2-induced FOXA1 binding sites. Genome browser tracks are normalized to a total of 10 million reads.

See also Figure S1.

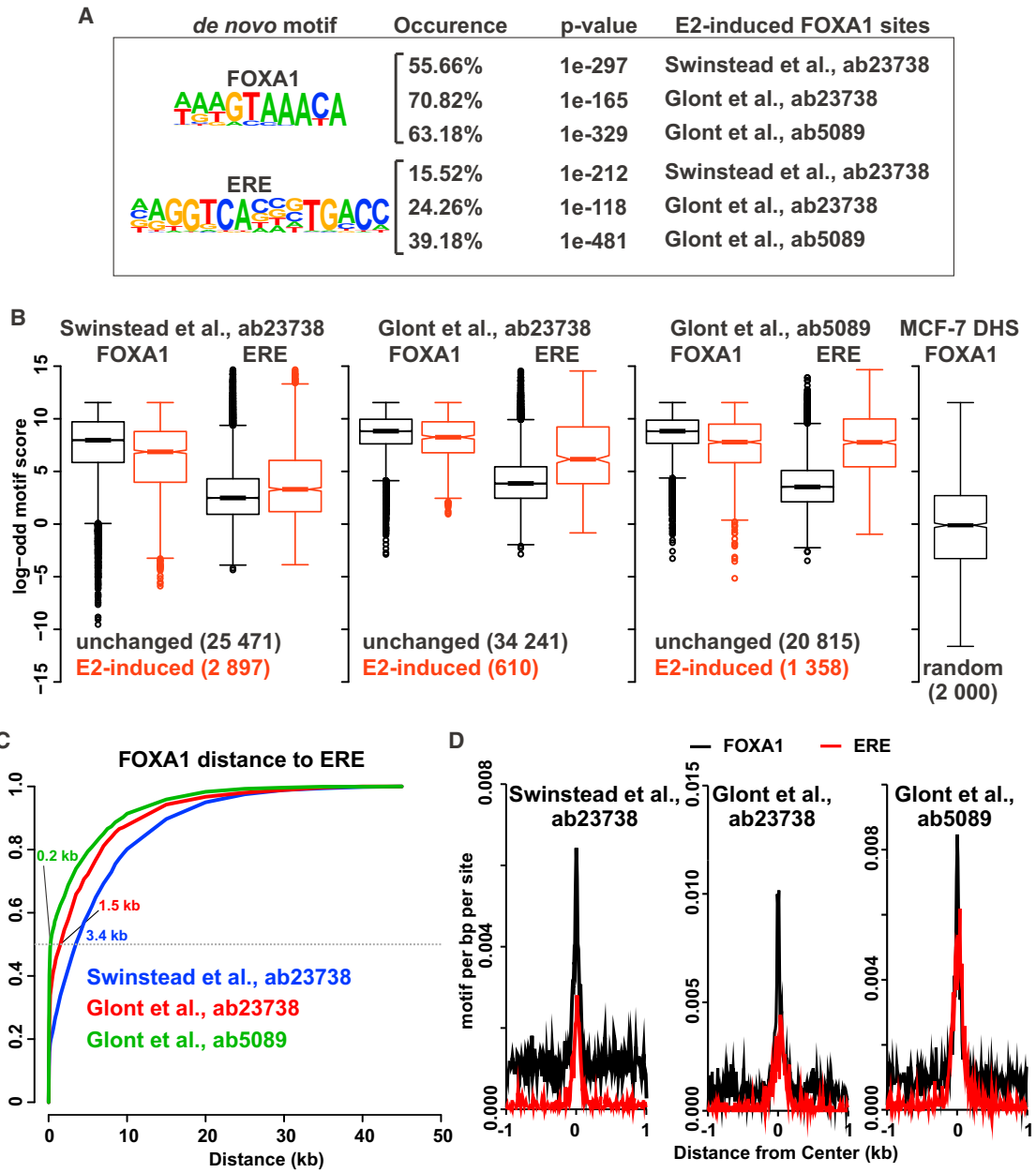

Figure 2. ERE and Forkhead Motifs Are Both Enriched at E2-Induced FOXA1 Sites in MCF-7 Cells

(A) *De novo* motif analysis of the ERE and FOXA1 motif enrichments at E2-induced FOXA1 sites from indicated datasets. Percentage of occurrence and motif enrichment p value are shown.

(B) Log-odd motif scores of FOXA1 or the ERE at unchanged (black) or E2-induced (red) FOXA1 sites from indicated datasets. Also displayed are FOXA1 motif scores from random DHSs in MCF-7 cells. Motif score distribution depicted as boxplots.

(C) Cumulative distribution function (CDF) of the distance between an E2-induced FOXA1 site and the closest ERE in indicated datasets. Median is depicted by gray dashed line, and median from each dataset is indicated with color coding.

(D) Aggregate plot of FOXA1 motif (black) and ERE (red) enrichment at E2-induced FOXA1 sites from indicated datasets. Plots are normalized to a total of 10 million reads and to motif per bp per site.

See also Figure S2.

motifs between unchanged and E2-induced FOXA1 sites. The motif score of FOXA1 was slightly lower in both MCF-7 (Figure 2B) and ZR-75-1 (Figure S2B) cells in E2-induced conditions, compared to unchanged FOXA1 sites. Regardless, most of the E2-induced sites displayed clearly higher FOXA1 motif scores, compared to random DNase hypersensitive sites (DHSs). The most striking difference was observed with the EREs that showed clearly higher motif scores in E2-induced compared to

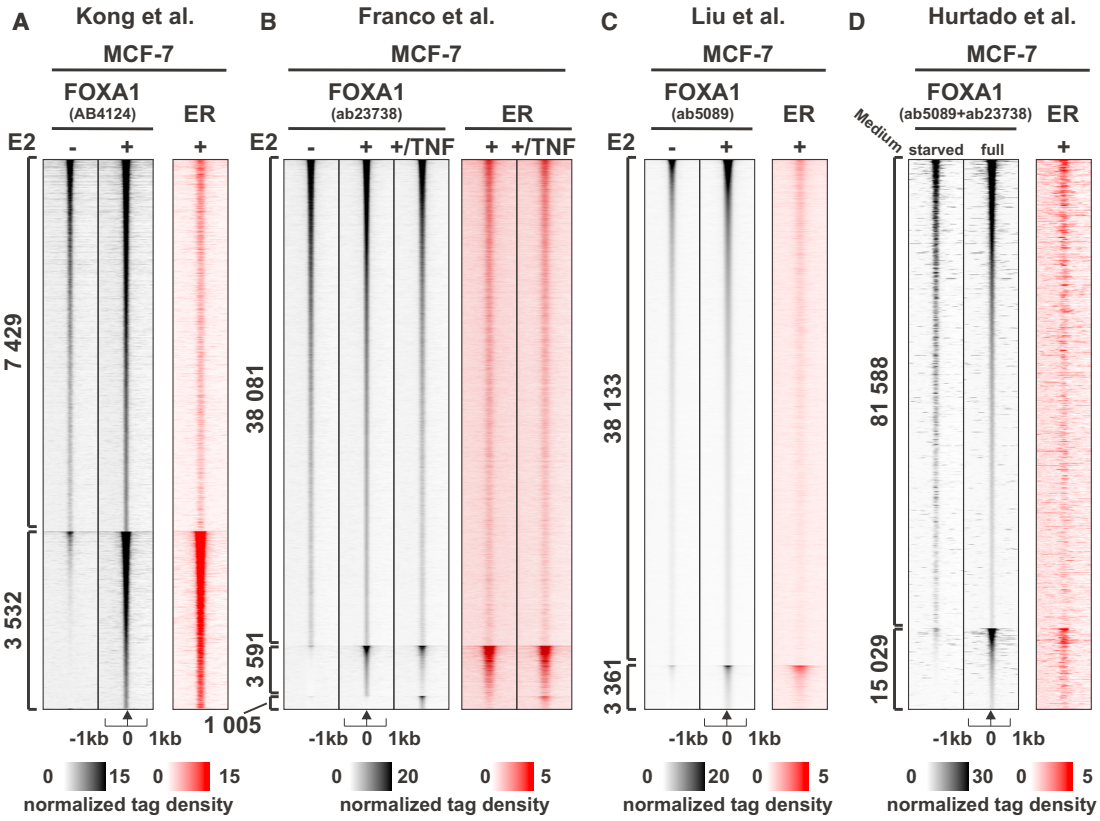

E

de novo motif	Occurence	p-value	E2/full media -induced FOXA1 sites
FOXA1	26.43%	1e-59	Kong et al., AB4124
	40.77%	1e-573	Franco et al., ab23738
	64.33%	1e-1563	Liu et al., ab5089
	52.92%	1e-2954	Hurtado et al., ab5089+ab23738
ERE	59.59%	1e-420	Kong et al., AB4124
	24.59%	1e-717	Franco et al., ab23738
	9.52%	1e-103	Liu et al., ab5089
	11.52%	1e-1323	Hurtado et al., ab5089+ab23738

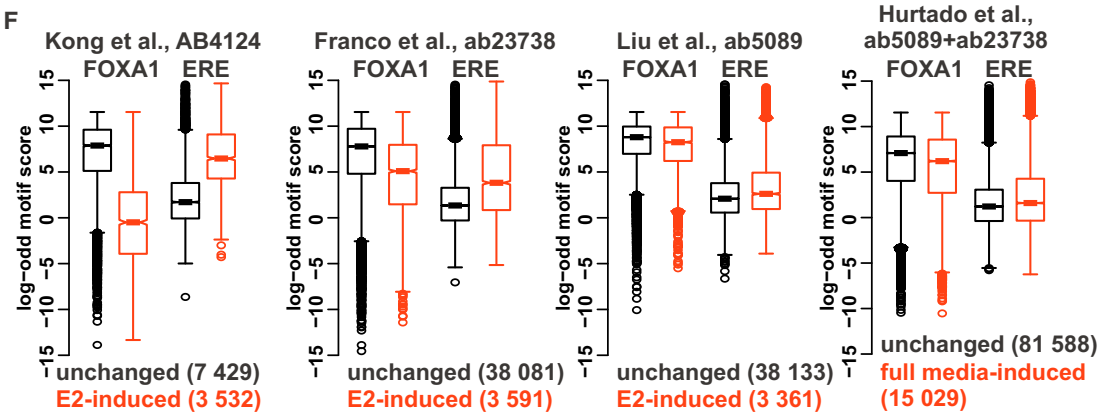

(legend on next page)

unchanged FOXA1 sites. These effects were seen with our (Swinstead et al., 2016) and with Glont et al. (2019) datasets. Interestingly, it has also been shown by the Myers laboratory that ER binding sites containing strong EREs are most often found at locations associated with closed chromatin (Gertz et al., 2013), and these sites open in response to E2 in a mode they term ''pioneering.'' This is in line with our original observation that ER binding induces the opening of chromatin, assisting the recruitment of FOXA1 (Swinstead et al., 2016). Thus, the striking enrichment of the ERE and FOXA1 motifs at the E2-induced FOXA1 sites further highlights the active role of the ER in reprogramming chromatin for subsequent FOXA1 accessibility.

If the ER reprograms chromatin for subsequent FOXA1 binding at these sites, the FOXA1 binding site should be in close linear proximity (i.e., *in cis*) to an ERE (Swinstead et al., 2016). We analyzed the distance between E2-induced FOXA1 sites to the closest ERE (see STAR Methods for details). In the MCF-7 cells, the median distance between an E2-induced FOXA1 site and an ERE was between 200 bp and 3.4 kb (Figure 2C), depending on the dataset. The median distance was even closer in the ZR-75-1 cells, ranging between 60 and 450 bp (Figure S2C), depending on the dataset. To aggregate these results, we assessed the ERE and forkhead motifs' enrichment at the E2-induced FOXA1 sites. Both cell lines in all datasets showed a clear enrichment of both the ERE and forkhead motifs at the center of the E2-induced FOXA1 sites (Figures 2D and S2D). In conclusion, our detailed motif analyses indicate that both the ERE and forkhead motifs are enriched at the E2-induced FOXA1 sites, suggesting that ''shadow'' binding events suggested by Carroll and colleagues (Glont et al. (2019) are based on inadequate motif analyses.

Datasets from Multiple Laboratories Indicate E2-Induced Binding of FOXA1

Although we observed E2-induced FOXA1 binding in both our and Glont et al. (2019) datasets, we wished to address these aspects more broadly, extending the analysis to all published experiments. Several other investigators have published FOXA1 ChIP-seq datasets in MCF-7 cells in the presence or absence of E2 (Franco et al., 2015; Kong et al., 2011; Liu et al., 2014). We re-analyzed these datasets, along with the original FOXA1 ChIP-seq data published by Carroll and colleagues (Hurtado et al., 2011) (see STAR Methods for details). Carroll and colleagues did not perform FOXA1 ChIP-seq in E2-treated MCF-7 cells; however, they did FOXA1 ChIP-seq experiments in starved versus full-media conditions (Hurtado et al., 2011). We used these as proxy for non-hormone treated conditions (starved) and E2-treated conditions (full media). FOXA1 ChIP-seq datasets from the Liu (Figure 3A) (Kong et al., 2011), Kraus (Figure 3B) (Franco et al., 2015), and Rosenfeld (Figure 3C) (Liu et al., 2014) laboratories showed a significant number of E2-induced FOXA1 sites. The E2-induced binding of FOXA1 can be observed from separate biological replicates (Figure S3A). Furthermore, all three laboratories had used different FOXA1 antibodies in their ChIP-seq experiments, indicating that an antibody epitope artifact is unlikely to explain the appearance of E2-induced FOXA1 sites. In addition, the original datasets from Carroll and colleagues showed over 15,000 full-media-induced FOXA1 binding events not present under hormone-starved conditions (Figure 3D). Again, ER binding was prevalent at all E2-induced FOXA1 binding sites, showing that ER reprogramming of FOXA1 binding can be observed from datasets generated by multiple investigators. Although the E2-induced FOXA1 sites have been disparaged in the past due to their relatively low signals (Zaret et al., 2016), it should be noted that the signal strength for both FOXA1 and the ER at the E2-induced sites can be very strong (Figure 3A). It should also be noted that simultaneous activation of the ER and p65 by a tumor necrosis factor (TNF) can result in additional FOXA1 binding events (Figure 3B) (Franco et al., 2015). This illustrates that other signal-dependent TFs can influence FOXA1 chromatin binding. Representative genome browser tracks are shown for all datasets (Figures S3B–S3E).

To complement our earlier conclusions, we performed similar motif analyses from all additional FOXA1 ChIP-seq datasets. As we observed earlier (Figure 2A), the ERE and forkhead motifs were both enriched at E2- and full-media-induced FOXA1 sites (Figure 3E). In addition, the motif score analysis of the ERE and FOXA1 motifs (Figure 3F) showed similar results, as observed earlier (Figure 2B). Although Kong et al. (2011) datasets showed a clear decrease in the FOXA1 motif scores between unchanged and E2-induced sites, the other datasets showed similar scores. Furthermore, the median distance between an E2-induced FOXA1 site and an ERE was between 600 bp and 3.1 kb (Figure S3F), depending on the dataset, which is similar to what was observed earlier (Figure 2C). Finally, all datasets (except Kong et al.) showed a clear enrichment of both the ERE and forkhead motifs at the center of the E2-induced FOXA1 sites (Figure S3G). In conclusion, E2-induced FOXA1 sites, as depicted in our original study (Swinstead et al., 2016), can be observed in all datasets representing five different laboratories.

Figure 3. Datasets from Several Different Laboratories Show E2-Induced Binding of FOXA1

(A–D) Heatmaps represent FOXA1 (black) and ER (red) ChIP-seq from Kong et al. (2011) (A), Franco et al. (2015) (B), Liu et al. (2014) (C), and Hurtado et al. (2011) (D). Unchanged FOXA1 sites are shown on top of the heatmap, and E2 and full-media-induced FOXA1 sites are on the bottom of the heatmap. Franco et al. (2015) (B) has E2+TNF-induced FOXA1 sites on the bottom of the heatmap. The number of binding sites is shown on the left of the heatmap. Each heatmap represents ±1 kb around the center of the FOXA1 peak. Binding intensity scale is noted below on a linear scale. Heatmaps are sorted based in FOXA1+E2/full-media binding intensity. All heatmaps are normalized to a total of 10 million reads and to tags per bp per site. Used FOXA1 antibody is depicted in the parentheses.

(E) *De novo* motif analysis of the ERE and FOXA1 motif enrichments at E2-induced FOXA1 sites from indicated datasets. Percentage of occurrence and motif enrichment p value are shown.

(F) Log-odd motif scores of FOXA1 or the ERE at unchanged (black) or E2-induced (red) FOXA1 sites from indicated datasets. Motif score distribution depicted as boxplots.

See also Figure S3.

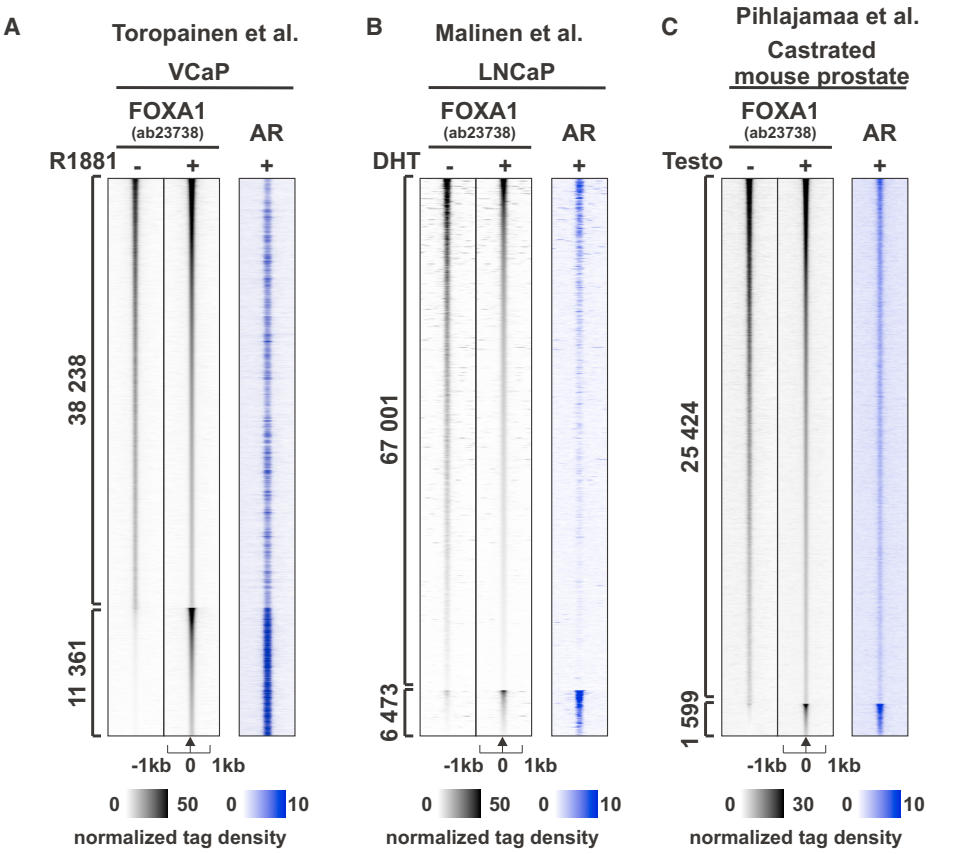

D

de novo motif	Occurence	p-value	Androgen-induced FOXA1 sites
FOXA1	58.79%	1e-1225	Toropainen et al., ab23738
	50.76%	1e-168	Malinen et al., ab23738
	48.72%	1e-381	Pihlajamaa et al., ab23738
ARE	53.95%	1e-2263	Toropainen et al., ab23738
	41.62%	1e-589	Malinen et al., ab23738
	27.27%	1e-308	Pihlajamaa et al., ab23738

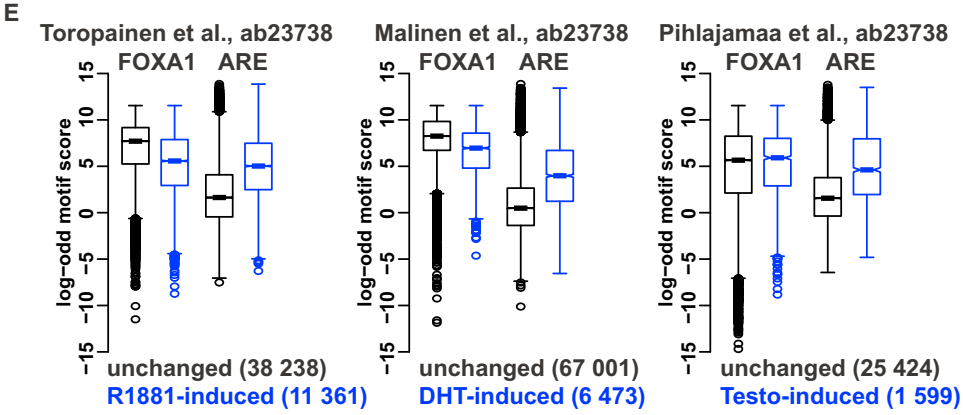

(legend on next page)

Androgen Receptor Activation Induces the Chromatin Binding of FOXA1 in Prostate Cancer Cells

Like the interplay between the ER and FOXA1 in breast cancer cells, the importance of FOXA1 in the regulation of the androgen receptor (AR) in prostate cancer cells has been extensively investigated (Pihlajamaa et al., 2015; Sahu et al., 2011). Carroll and colleagues have suggested that AR binding is regulated by FOXA1 in an asymmetrical fashion (Lupien et al., 2008; Robinson et al., 2014). However, depletion of FOXA1 from prostate cancer cells influences only a subset of AR chromatin binding (Sahu et al., 2011). This suggests that the AR could reprogram FOXA1 binding to chromatin, like the ER in breast cancer cells. To assess this, we re-analyzed available FOXA1 ChIP-seq datasets (see STAR Methods for details) generated from prostate cancer cells treated with or without androgens (Malinen et al., 2017; Toropainen et al., 2015). In addition, we re-analyzed FOXA1 ChIP-seq datasets generated from castrated mouse prostates treated with or without androgens (Pihlajamaa et al., 2014). Androgens induced the chromatin binding of FOXA1 in human vertebral cancer of the prostate (VCaP; Figure 4A) and lymph node carcinoma of the prostate (LNCaP; Figure 4B) cells and in castrated mouse prostates (Figure 4C). The androgen-induced binding of FOXA1 can be observed from separate biological replicates (Figure S4A). Especially prevalent are the over 11,000 R1881-induced FOXA1 binding sites in VCaP cells, where the FOXA1 signal strength is similar to the remaining ~38,000 sites. The AR-dependent FOXA1 binding sites were highly enriched with AR binding showing the strongest receptor binding. Strong AR binding was also observed at induced FOXA1 sites in LNCaP and mouse prostate datasets. Representative genome browser tracks are shown for all datasets (Figures S4B–S4D).

To complement our ER observations, we performed motif analyses from FOXA1 datasets generated from prostate cancer cells or mouse prostates. As observed with ER data earlier (Figures 2A and 3E), the androgen response element (ARE) and forkhead motifs were both enriched at androgen-induced FOXA1 sites (Figure 4D). In addition, the motif score analysis of the ARE and FOXA1 motifs (Figure 4E) showed similar results to those observed with the ER earlier (Figures 2B and 3F). Furthermore, the median distance between an androgen-induced FOXA1 site and an ARE was between 1 and 3.0 kb (Figure S4E), depending on the dataset. This was similar to what was observed with the ER data (Figures 2C and S3F). Finally, all datasets showed a clear enrichment of both the ARE and the forkhead motifs at the center of the androgen-induced FOXA1 sites (Figure S4F). In conclusion, the reprogramming of FOXA1 chromatin binding is observed with multiple SRs, in multiple cell lines, with datasets generated by multiple investigators.

DISCUSSION

The idea of pioneering descends from the concept of master TFs first developed in the 1980s. Early examples include Myo-D (Davis et al., 1987) and the regulatory genes of the bithorax complex (Lewis, 1985). In the original thinking (Ohno, 1979), master regulators were proposed as genetic elements selected during evolution to serve as controlling elements in a given developmental pathway. The elements could include factors with a variety of activities, not necessarily TFs. With the realization in the mid-80s of the importance of chromatin as a barrier to TF access, the penetration of closed chromatin became a key issue to the understanding of selective TF binding to the genome, and the concept of "pioneer factors" eventually emerged (Cirillo et al., 2002).

Thus, two central issues arise concerning the alternate views of pioneering by SRs, or any set of factors: Are these factors chosen early in the evolution of genetic networks from a primitive set of factors, or are they selected based on a specific property (i.e., a special ability to invade chromatin)? For the SRs, this issue acquired a special prominence with the reports that FOXA1 was a frequent initiating factor for ER action in breast cancer (Carroll et al., 2005), suggesting a potentially new target for therapy with this important disease. With further study (Carroll et al., 2006; Lupien et al., 2008), the concept developed that FOXA1 is an obligate pioneer for ER binding (Zaret and Carroll, 2011). A corollary of this model is that the ER and the other SRs are unable to invade chromatin without the assistance of a pioneer factor (Iwafuchi-Doi et al., 2016).

For an unbiased approach to the issue, we have addressed here many SR datasets that bear on the question. To be considered, such data must include deep sequencing for chromatin opening (DNase-seq, ATAC-seq) and parallel high-quality ChIP-seq analyses. Looking at the totality of the data, it is clear that the ER, GR, and AR can each serve as initiating factors to open chromatin and, in a significant subset of events, induce the recruitment of the FOXA1 pioneer. In this mode, FOXA1 is essentially serving as a cofactor for the receptors (Figure 5A). We introduced the term "initiating factor" to describe chromatin penetration by the SRs as a symmetric process. That is, the role of initiator among two or more factors can switch, depending on the local chromatin conformation (Voss et al., 2011). This line of reasoning would be in concordance with the recently introduced

Figure 4. The AR Induces the Chromatin Binding of FOXA1 in Prostate Cancer Cells and in the Mouse Prostate

(A–C) Heatmaps represent FOXA1 (black) and AR (blue) ChIP-seq from Toropainen et al. (2015) (A), Malinen et al. (2017) (B), and Pihlajamaa et al. (2014) (C). Unchanged FOXA1 sites are shown on top of the heatmap, and androgen-induced FOXA1 sites are on the bottom of the heatmap. The cells were treated by Toropainen et al. (2015) with metribolone (R1881), by Malinen et al. (2017) with dihydrotestosterone (DHT), and by Pihlajamaa et al. (2014) with testosterone (Testo). The number of binding sites is shown on the left of the heatmap. Each heatmap represents ±1 kb around the center of the FOXA1 peak. Binding intensity scale is noted below on a linear scale. Heatmaps are sorted based on FOXA1+androgen binding intensity. All heatmaps are normalized to a total of 10 million reads and to tags per bp per site. Used FOXA1 antibody is depicted in the parentheses.

(D) *De novo* motif analysis of the ARE and FOXA1 motif enrichment at androgen-induced FOXA1 sites from indicated datasets. Percentage of occurrence and motif enrichment p value are shown.

(E) Log-odd motif scores of FOXA1 or ARE at unchanged (black) or androgen-induced (blue) FOXA1 sites from indicated datasets. Motif score distribution depicted as boxplots.

See also Figure S4.

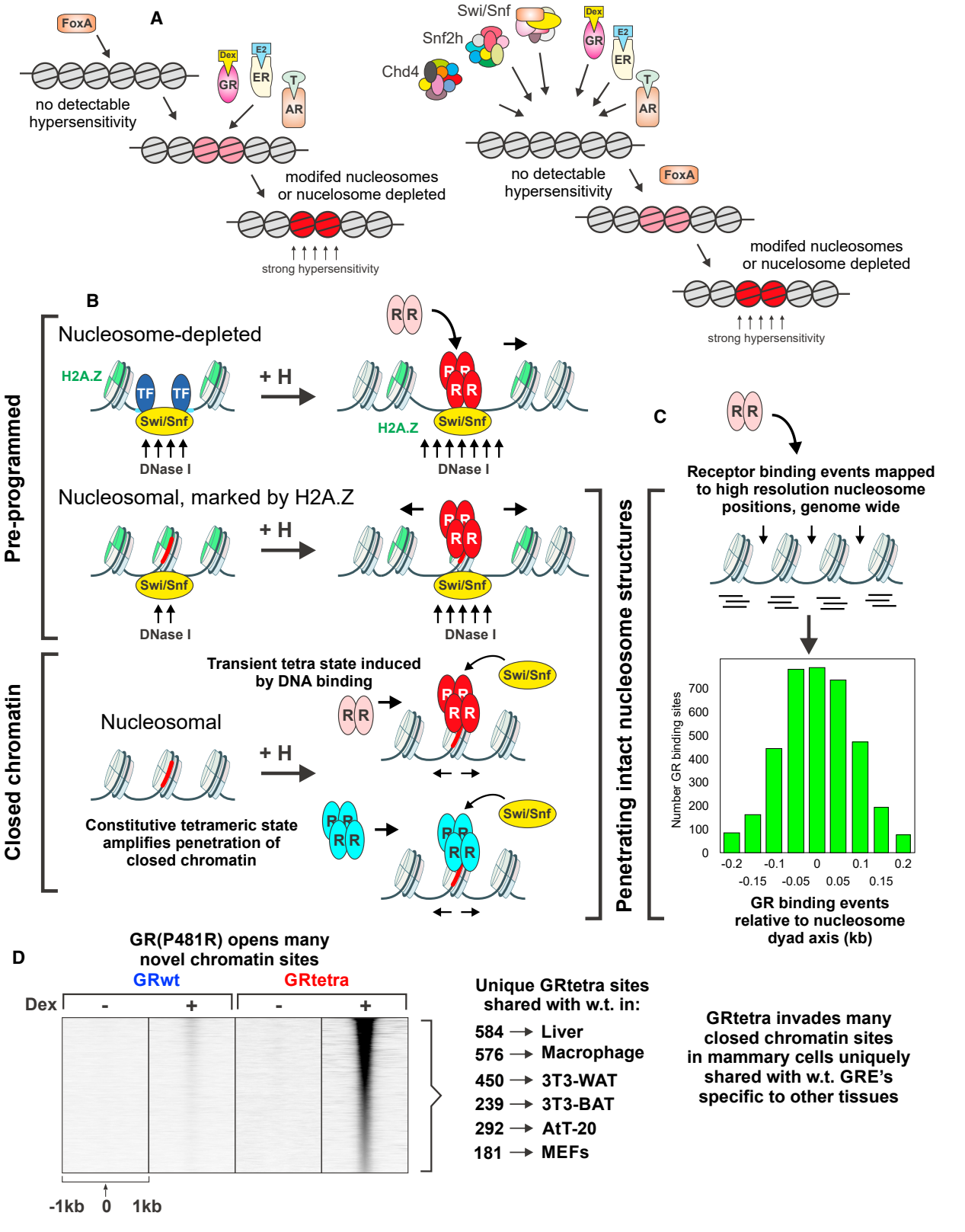

(legend on next page)

concept that there are a variety of nucleosome attack modes, and a clear demarcation between pioneer and cofactor may be too extreme (Zhu et al., 2018).

A New Wrinkle

Two recent studies shed new light on the issue of chromatin opening by SRs. GR binding events were profiled on high-resolution nucleosome positioning data genome-wide (Johnson et al., 2018). In mammalian cells, this type of data requires very deep sequencing and has been rarely attempted. The GR sites were characterized in three general states (Figure 5B): (1) the most accessible sites are nucleosome depleted, with the BRG1 (SMARCA4) ATP-dependent remodeling complex preloaded on the site, presumably by other factors; (2) a second class of sites, less accessible, are nucleosomal but marked by the H2A.Z variant histone and again harbor BRG1; and (3) the third class of sites are nucleosomal, with no evidence of nuclease accessibility (see Figure S5). In this third class, the GR is a true initiating factor, recruiting BRG1 and opening chromatin. In this study, it was also found that GR binding on nucleosomal sites (classes 2 and 3) was predominantly centered on the nucleosome dyad (Figure 5C). This discovery stands in contrast to the frequent assertion that "non-pioneer" factor binding is largely limited to nucleosome edges or inter-nucleosomal regions (Klemm et al., 2019; Thurman et al., 2012). Thus, the GR frequently binds to the double gyres on an intact nucleosome surface during the initiator step. This finding is quite striking and in line with the original observation (Perlmann and Wrange, 1988) that a purified GR can bind to a reconstituted nucleosome.

A second study (Paakinaho et al., 2019) introduces a new "wrinkle" to the chromatin opening story. Using live cell fluorescence correlation spectroscopy methods, Presman and colleagues reported in 2016 that GR-response element binding induces tetramerization of the receptor (Presman et al., 2016). Yamamoto and colleagues had earlier developed the concept that DNA binding introduces an allosteric transition in the receptor that could alter its cofactor interactions (van Tilborg et al., 2000). During this work, they isolated a GR DNA binding domain mutation that mimicked the DNA-bound conformation. Introducing this mutation in the full-length receptor (called GRtetra) was found to create a "super receptor," able to penetrate many sites in mammary cells (Figure 5D) not available to the wild-type receptor (Paakinaho et al., 2019). The vast majority of these new sites correspond to glucocorticoid response elements (GREs) bound by the wild-type receptor in cells from other tissue types. That is, the GRtetra receptor overcomes chromatin repression in mammary cells and pioneers authentic sites specific to other tissues. The working model from this study argues that the DNA-induced receptor transition is a normal but transient process, which in some cases allows the receptor to initiate chromatin opening. Conversion of the receptor to the constitutive DNA-bound form (Figure 5B) amplifies the ability of the mutant receptor to penetrate and open closed chromatin, the "initiator" activity.

Conclusions

A careful examination of all datasets relevant to chromatin binding by SRs documents the general ability of these factors as a group to initiate the process of chromatin opening and, in some cases, recruit the FOXA1 protein as a cofactor. It is likely more accurate to consider this process (referred to as the initiator activity) as one of many chromatin attack modes that may involve a wide variety of TFs, rather than the arbitrary division of factors as "pioneers" and "followers." To date, essentially all treatments of this issue involve static datasets from dead cells and large cell populations. A rigorous approach to this central "who is first" question in gene expression biology will require work that addresses the process in real time in living cells. Fortunately, recent developments in high-resolution single-molecule microscopy offer great promise on this front. The issue of sequence of arrival has not yet been addressed but will likely be tackled in the near future.

STAR★METHODS

Detailed methods are provided in the online version of this paper and include the following:

- KEY RESOURCES TABLE
- LEAD CONTACT AND MATERIALS AVAILABILITY
- METHOD DETAILS
- QUANTIFICATION AND STATISTICAL ANALYSIS
- DATA AND CODE AVAILABILITY

SUPPLEMENTAL INFORMATION

Supplemental Information can be found online at https://doi.org/10.1016/j.celrep.2019.08.039.

Figure 5. Steroid Receptor Binding to Chromatin

(A) FoxA1 serves as a pioneer factor for steroid receptors at some closed chromatin sites (left). Secondary binding of the receptors recruits other activities that increase the nuclease accessibility of the sites. At other sites, attack on the closed region is initiated directly by the SR, creating accessible regions in concert with ATP-dependent remodeling systems (right).

(B) Glucocorticoid receptor binds chromatin in three modes (Johnson et al., 2018). Preprogrammed regions contain open chromatin depleted of nucleosomes or nuclease accessible sites with nucleosomes containing variant and otherwise modified histones. Closed regions contain intact nucleosomes with no detectable nuclease accessibility (see Figure S5). Live cell studies show that the GR binds to some GREs as tetramers (Presman et al., 2016). This DNA-induced transition is constitutively induced by the P481R mutation (GRtetra) that has been shown to mimic the DNA-bound form of the GR DNA binding domain (Presman et al., 2016).

(C) High-resolution nucleosome mapping combined with ChIP-seq reveals a preponderance of GR binding clustered around the nucleosome dyad axis (Johnson et al., 2018).

(D) The GRtetra invades many more closed chromatin sites than the wild-type receptor. These sites correspond to tissue-specific sites that are closed in mammary cells but available to wild-type receptors in other cell types (Paakinaho et al., 2019).

See also Figure S5.

ACKNOWLEDGMENTS

V.P. was supported by the Academy of Finland and the Sigrid Jusélius Foundation. E.E.S. was supported by the Office of the Assistant Secretary of Defense for Health Affairs through the Breast Cancer Research Program under award W81XWH-17-1-0067. Opinions, interpretations, conclusions, and recommendations are those of the author and are not necessarily endorsed by the Department of Defense. D.M.P. was supported by CONICET and the ANPCyT (PICT 2017-0850). L.G. was supported by the Independent Research Fund Denmark and the Danish National Research Foundation. G.L.H. was supported by the Intramural Research Program of the CCR, NCI, NIH.

AUTHOR CONTRIBUTIONS

V.P. analyzed the data with contributions from E.E.S., D.M.P., and L.G. G.L.H. directed the project. All authors participated in the writing of the manuscript.

DECLARATION OF INTERESTS

The authors declare no competing interests.

Received: May 15, 2019
Revised: August 8, 2019
Accepted: August 12, 2019
Published: September 17, 2019

REFERENCES

Archer, T.K., Cordingley, M.G., Wolford, R.G., and Hager, G.L. (1991). Transcription factor access is mediated by accurately positioned nucleosomes on the mouse mammary tumor virus promoter. Mol. Cell. Biol. *11*, 688–698.

Ben-David, U., Siranosian, B., Ha, G., Tang, H., Oren, Y., Hinohara, K., Strathdee, C.A., Dempster, J., Lyons, N.J., Burns, R., et al. (2018). Genetic and transcriptional evolution alters cancer cell line drug response. Nature *560*, 325–330.

Carroll, J.S., Liu, X.S., Brodsky, A.S., Li, W., Meyer, C.A., Szary, A.J., Eeckhoute, J., Shao, W., Hestermann, E.V., Geistlinger, T.R., et al. (2005). Chromosome-wide mapping of estrogen receptor binding reveals long-range regulation requiring the forkhead protein FoxA1. Cell *122*, 33–43.

Carroll, J.S., Meyer, C.A., Song, J., Li, W., Geistlinger, T.R., Eeckhoute, J., Brodsky, A.S., Keeton, E.K., Fertuck, K.C., Hall, G.F., et al. (2006). Genome-wide analysis of estrogen receptor binding sites. Nat. Genet. *38*, 1289–1297.

Chen, T. (2008). Nuclear receptor drug discovery. Curr. Opin. Chem. Biol. *12*, 418–426.

Cirillo, L.A., McPherson, C.E., Bossard, P., Stevens, K., Cherian, S., Shim, E.Y., Clark, K.L., Burley, S.K., and Zaret, K.S. (1998). Binding of the winged-helix transcription factor HNF3 to a linker histone site on the nucleosome. EMBO J. *17*, 244–254.

Cirillo, L.A., Lin, F.R., Cuesta, I., Friedman, D., Jarnik, M., and Zaret, K.S. (2002). Opening of compacted chromatin by early developmental transcription factors HNF3 (FoxA) and GATA-4. Mol. Cell *9*, 279–289.

Davis, R.L., Weintraub, H., and Lassar, A.B. (1987). Expression of a single transfected cDNA converts fibroblasts to myoblasts. Cell *51*, 987–1000.

Donaghey, J., Thakurela, S., Charlton, J., Chen, J.S., Smith, Z.D., Gu, H., Pop, R., Clement, K., Stamenova, E.K., Karnik, R., et al. (2018). Genetic determinants and epigenetic effects of pioneer-factor occupancy. Nat. Genet. *50*, 250–258.

Franco, H.L., Nagari, A., and Kraus, W.L. (2015). TNFα signaling exposes latent estrogen receptor binding sites to alter the breast cancer cell transcriptome. Mol. Cell *58*, 21–34.

Gertz, J., Savic, D., Varley, K.E., Partridge, E.C., Safi, A., Jain, P., Cooper, G.M., Reddy, T.E., Crawford, G.E., and Myers, R.M. (2013). Distinct properties of cell-type-specific and shared transcription factor binding sites. Mol. Cell *52*, 25–36.

Glont, S.E., Chernukhin, I., and Carroll, J.S. (2019). Comprehensive Genomic Analysis Reveals that the Pioneering Function of FOXA1 Is Independent of Hormonal Signaling. Cell Rep. *26*, 2558–2565.e3.

Grøntved, L., John, S., Baek, S., Liu, Y., Buckley, J.R., Vinson, C., Aguilera, G., and Hager, G.L. (2013). C/EBP maintains chromatin accessibility in liver and facilitates glucocorticoid receptor recruitment to steroid response elements. EMBO J. *32*, 1568–1583.

He, X., Chatterjee, R., John, S., Bravo, H., Sathyanarayana, B.K., Biddie, S.C., FitzGerald, P.C., Stamatoyannopoulos, J.A., Hager, G.L., and Vinson, C. (2013). Contribution of nucleosome binding preferences and co-occurring DNA sequences to transcription factor binding. BMC Genomics *14*, 428.

Heinz, S., Benner, C., Spann, N., Bertolino, E., Lin, Y.C., Laslo, P., Cheng, J.X., Murre, C., Singh, H., and Glass, C.K. (2010). Simple combinations of lineage-determining transcription factors prime cis-regulatory elements required for macrophage and B cell identities. Mol. Cell *38*, 576–589.

Hoffman, J.A., Trotter, K.W., Ward, J.M., and Archer, T.K. (2018). BRG1 governs glucocorticoid receptor interactions with chromatin and pioneer factors across the genome. eLife *7*, e35073.

Hurtado, A., Holmes, K.A., Ross-Innes, C.S., Schmidt, D., and Carroll, J.S. (2011). FOXA1 is a key determinant of estrogen receptor function and endocrine response. Nat. Genet. *43*, 27–33.

Iwafuchi-Doi, M., Donahue, G., Kakumanu, A., Watts, J.A., Mahony, S., Pugh, B.F., Lee, D., Kaestner, K.H., and Zaret, K.S. (2016). The Pioneer Transcription Factor FoxA Maintains an Accessible Nucleosome Configuration at Enhancers for Tissue-Specific Gene Activation. Mol. Cell *62*, 79–91.

Johnson, T.A., Chereji, R.V., Stavreva, D.A., Morris, S.A., Hager, G.L., and Clark, D.J. (2018). Conventional and pioneer modes of glucocorticoid receptor interaction with enhancer chromatin in vivo. Nucleic Acids Res. *46*, 203–214.

King, H.W., and Klose, R.J. (2017). The pioneer factor OCT4 requires the chromatin remodeller BRG1 to support gene regulatory element function in mouse embryonic stem cells. eLife *6*, e22631.

Klemm, S.L., Shipony, Z., and Greenleaf, W.J. (2019). Chromatin accessibility and the regulatory epigenome. Nat. Rev. Genet. *20*, 207–220.

Kong, S.L., Li, G., Loh, S.L., Sung, W.K., and Liu, E.T. (2011). Cellular reprogramming by the conjoint action of ERα, FOXA1, and GATA3 to a ligand-inducible growth state. Mol. Syst. Biol. *7*, 526.

Langmead, B., Trapnell, C., Pop, M., and Salzberg, S.L. (2009). Ultrafast and memory-efficient alignment of short DNA sequences to the human genome. Genome Biol. *10*, R25.

Lewis, E.B. (1985). Regulation of the genes of the bithorax complex in Drosophila. Cold Spring Harb. Symp. Quant. Biol. *50*, 155–164.

Liu, Z., Merkurjev, D., Yang, F., Li, W., Oh, S., Friedman, M.J., Song, X., Zhang, F., Ma, Q., Ohgi, K.A., et al. (2014). Enhancer activation requires trans-recruitment of a mega transcription factor complex. Cell *159*, 358–373.

Love, M.I., Huber, W., and Anders, S. (2014). Moderated estimation of fold change and dispersion for RNA-seq data with DESeq2. Genome Biol. *15*, 550.

Lupien, M., Eeckhoute, J., Meyer, C.A., Wang, Q., Zhang, Y., Li, W., Carroll, J.S., Liu, X.S., and Brown, M. (2008). FoxA1 translates epigenetic signatures into enhancer-driven lineage-specific transcription. Cell *132*, 958–970.

Malinen, M., Niskanen, E.A., Kaikkonen, M.U., and Palvimo, J.J. (2017). Crosstalk between androgen and pro-inflammatory signaling remodels androgen receptor and NF-κB cistrome to reprogram the prostate cancer cell transcriptome. Nucleic Acids Res. *45*, 619–630.

Mayran, A., and Drouin, J. (2018). Pioneer transcription factors shape the epigenetic landscape. J. Biol. Chem. *293*, 13795–13804.

Miranda, T.B., Voss, T.C., Sung, M.H., Baek, S., John, S., Hawkins, M., Grøntved, L., Schiltz, R.L., and Hager, G.L. (2013). Reprogramming the chromatin landscape: interplay of the estrogen and glucocorticoid receptors at the genomic level. Cancer Res. *73*, 5130–5139.

Ohno, S. (1979). Major Sex-Determining Genes*Volume 11* (Springer Verlag).

Paakinaho, V., Johnson, T.A., Presman, D.M., and Hager, G.L. (2019). Glucocorticoid receptor quaternary structure drives chromatin occupancy and transcriptional outcome. Genome Res. *29*, 1223–1234.

Perlmann, T., and Wrange, O. (1988). Specific glucocorticoid receptor binding to DNA reconstituted in a nucleosome. EMBO J. *7*, 3073–3079.

Pihlajamaa, P., Sahu, B., Lyly, L., Aittomäki, V., Hautaniemi, S., and Jänne, O.A. (2014). Tissue-specific pioneer factors associate with androgen receptor cistromes and transcription programs. EMBO J. *33*, 312–326.

Pihlajamaa, P., Sahu, B., and Jänne, O.A. (2015). Determinants of Receptor- and Tissue-Specific Actions in Androgen Signaling. Endocr. Rev. *36*, 357–384.

Presman, D.M., Ganguly, S., Schiltz, R.L., Johnson, T.A., Karpova, T.S., and Hager, G.L. (2016). DNA binding triggers tetramerization of the glucocorticoid receptor in live cells. Proc. Natl. Acad. Sci. USA *113*, 8236–8241.

Richard-Foy, H., and Hager, G.L. (1987). Sequence-specific positioning of nucleosomes over the steroid-inducible MMTV promoter. EMBO J. *6*, 2321–2328.

Robinson, M.D., McCarthy, D.J., and Smyth, G.K. (2010). edgeR: a Bioconductor package for differential expression analysis of digital gene expression data. Bioinformatics *26*, 139–140.

Robinson, J.T., Thorvaldsdóttir, H., Winckler, W., Guttman, M., Lander, E.S., Getz, G., and Mesirov, J.P. (2011). Integrative genomics viewer. Nat. Biotechnol. *29*, 24–26.

Robinson, J.L., Hickey, T.E., Warren, A.Y., Vowler, S.L., Carroll, T., Lamb, A.D., Papoutsoglou, N., Neal, D.E., Tilley, W.D., and Carroll, J.S. (2014). Elevated levels of FOXA1 facilitate androgen receptor chromatin binding resulting in a CRPC-like phenotype. Oncogene *33*, 5666–5674.

Sahu, B., Laakso, M., Ovaska, K., Mirtti, T., Lundin, J., Rannikko, A., Sankila, A., Turunen, J.P., Lundin, M., Konsti, J., et al. (2011). Dual role of FoxA1 in androgen receptor binding to chromatin, androgen signalling and prostate cancer. EMBO J. *30*, 3962–3976.

Swinstead, E.E., Miranda, T.B., Paakinaho, V., Baek, S., Goldstein, I., Hawkins, M., Karpova, T.S., Ball, D., Mazza, D., Lavis, L.D., et al. (2016). Steroid Receptors Reprogram FoxA1 Occupancy through Dynamic Chromatin Transitions. Cell *165*, 593–605.

Takaku, M., Grimm, S.A., Shimbo, T., Perera, L., Menafra, R., Stunnenberg, H.G., Archer, T.K., Machida, S., Kurumizaka, H., and Wade, P.A. (2016). GATA3-dependent cellular reprogramming requires activation-domain dependent recruitment of a chromatin remodeler. Genome Biol. *17*, 36.

Thurman, R.E., Rynes, E., Humbert, R., Vierstra, J., Maurano, M.T., Haugen, E., Sheffield, N.C., Stergachis, A.B., Wang, H., Vernot, B., et al. (2012). The accessible chromatin landscape of the human genome. Nature *489*, 75–82.

Toropainen, S., Malinen, M., Kaikkonen, S., Rytinki, M., Jääskeläinen, T., Sahu, B., Jänne, O.A., and Palvimo, J.J. (2015). SUMO ligase PIAS1 functions as a target gene selective androgen receptor coregulator on prostate cancer cell chromatin. Nucleic Acids Res. *43*, 848–861.

van Tilborg, M.A., Lefstin, J.A., Kruiskamp, M., Teuben, J., Boelens, R., Yamamoto, K.R., and Kaptein, R. (2000). Mutations in the glucocorticoid receptor DNA-binding domain mimic an allosteric effect of DNA. J. Mol. Biol. *301*, 947–958.

Voss, T.C., Schiltz, R.L., Sung, M.H., Yen, P.M., Stamatoyannopoulos, J.A., Biddie, S.C., Johnson, T.A., Miranda, T.B., John, S., and Hager, G.L. (2011). Dynamic exchange at regulatory elements during chromatin remodeling underlies assisted loading mechanism. Cell *146*, 544–554.

Zaret, K.S., and Carroll, J.S. (2011). Pioneer transcription factors: establishing competence for gene expression. Genes Dev. *25*, 2227–2241.

Zaret, K.S., Lerner, J., and Iwafuchi-Doi, M. (2016). Chromatin Scanning by Dynamic Binding of Pioneer Factors. Mol. Cell *62*, 665–667.

Zhu, F., Farnung, L., Kaasinen, E., Sahu, B., Yin, Y., Wei, B., Dodonova, S.O., Nitta, K.R., Morgunova, E., Taipale, M., et al. (2018). The interaction landscape between transcription factors and the nucleosome. Nature *562*, 76–81.

STAR★METHODS

KEY RESOURCES TABLE

REAGENT or RESOURCE	SOURCE	IDENTIFIER
Deposited Data		
FoxA1 and ER ChIP-seq, and DNase-seq from MCF-7 and ZR-75-1 cells	Swinstead et al., 2016	GEO: GSE72249
FoxA1 ChIP-seq from MCF-7 and ZR-75-1 cells	Glont et al., 2019	GEO: GSE112969
FoxA1 and ER ChIP-seq from MCF-7 cells	Kong et al., 2011	GEO: GSE26831; GEO: GSE23893
FoxA1 and ER ChIP-seq from MCF-7 cells	Franco et al., 2015	GEO: GSE59530
FoxA1 and ER ChIP-seq from MCF-7 cells	Liu et al., 2014	GEO: GSE60272
FoxA1 and ER ChIP-seq from MCF-7 cells	Hurtado et al., 2011	GEO: GSE25710
FoxA1 and AR ChIP-seq from VCaP cells	Toropainen et al., 2015	GEO: GSE56086
FoxA1 and AR ChIP-seq from LNCaP cells	Malinen et al., 2017	GEO: GSE83860
FoxA1 and AR ChIP-seq from castrated mouse prostate	Pihlajamaa et al., 2014	GEO: GSE47192
Software and Algorithms		
FastQC 0.11.7	NA	https://www.bioinformatics.babraham.ac.uk/projects/fastqc/; RRID:SCR_014583
FASTX-toolkit 0.0.13	NA	http://hannonlab.cshl.edu/fastx_toolkit/; RRID:SCR_005534
Bowtie 0.12.7	Langmead et al., 2009	http://bowtie-bio.sourceforge.net/index.shtml; RRID:SCR_005476
HOMER 4.10	Heinz et al., 2010	http://homer.ucsd.edu/homer/; RRID:SCR_010881
IGV 2.3	Robinson et al., 2011	http://software.broadinstitute.org/software/igv/home; RRID:SCR_011793

LEAD CONTACT AND MATERIALS AVAILABILITY

Further information and requests for resources and reagents should be directed to and will be fulfilled by the Lead Contact, Gordon L. Hager (hagerg@dce41.nci.nih.gov). This study did not generate new unique reagents.

METHOD DETAILS

Downloaded raw fastq data were quality checked and filtered using FastQC 0.11.7 (https://www.bioinformatics.babraham.ac.uk/projects/fastqc/) and FASTX-toolkit 0.0.13 (http://hannonlab.cshl.edu/fastx_toolkit/) with -q 10, -p 97 and duplicate reads collapsed before alignment of reads against the human genome (hg19) or mouse genome (mm10) using bowtie 0.12.7 (http://bowtie-bio.sourceforge.net/index.shtml) (Langmead et al., 2009), allowing only one mismatch and accepting only the best alignment. Subsequent downstream analyses were performed with HOMER 4.10 (http://homer.ucsd.edu/homer/) (Heinz et al., 2010).

Tag directories were generated using makeTagDirectory with default parameters from each individual replicate. ChIP-seq peak calling was performed using findPeaks with default parameters (FDR < 0.001, fold over control > 4, fold over local background > 4) using style factor for both FOXA1 and steroid receptor ChIP-seq data. The control sample chosen for each individual sample was either from the same dataset or from the same laboratory. Details are provided in Table S1. To obtain replicate concordant peaks, called peaks from each individual replicate sample were overlapped. Concordant peaks had to overlap at least 1 bp to be called concordant. Hormone-induced FOXA1 binding sites were determined using getDifferentialPeaks using Poisson p value (< 0.001) and fold over untreated (> 3 or > 4) as cutoffs. Fold over untreated depended on the dataset, with > 3 for Glont et al., Liu et al., Hurtado et al., Malinen et al., Pihlajamaa et al., and > 4 with Swinstead et al., Kong et al., Franco et al., and Toropainen et al. datasets. For determination combined tag directory from each replicate sample was used. To check the hormone-induced FOXA1 binding sites from each biological replicate sample, normalized log2 tag density from each replicate was extracted. This was done for all datasets with biological replicate experiments. Distribution of log2 tag density for each biological replicate was shown as Tukey boxplot with notches depicting the confidence of the median. Outliers were not shown. Heatmaps were generated

using annotatePeaks with size ± 1kb with 20 bp bins. Generated heatmaps were normalized to 10 million mapped reads and to tags per bp per site. Data were sorted based on signal intensity of FOXA1+hormone sample before visualization. Genome browser tracks were generated from combined tag directory using makeUCSCfile, converting the obtained bedGraph to TDF using igvtool and visualized with IGV 2.3 (http://software.broadinstitute.org/software/igv/home) (Robinson et al., 2011). *De novo* motif analysis was performed using findMotifsGenome with defaults parameters. Log-odd motif scores were determined with annotatePeaks using foxa1.mcf7.motif, and ere.motif or are.motif. For determination of FOXA1 motif scores from random DHS, 2 000 sites were randomly selected from all DHS identified from MCF-7 or ZR-75-1 cells. DHS determination was performed as ChIP-seq peak calling using HOMER. Distribution of scores was shown as Tukey boxplot with notches depicting the confidence of the median. The distance between hormone-induced FOXA1 site and closest ERE/ARE was determined using annotatePeaks with ere.motif or are.motif. CDF was calculated based on the individual distances. Aggregate plots of FOXA1 motif and ERE/ARE were generated using annotatePeaks with size ± 1kb with 10 bp bins. Generated aggregate plots were normalized to 10 million mapped reads and to motif per bp per site.

QUANTIFICATION AND STATISTICAL ANALYSIS

Analysis details are provided above in Method Details section, and in the figures and figure legends.

DATA AND CODE AVAILABILITY

This study did not generate any new datasets or code. The following published original ChIP-seq datasets were used in the analyses: Swinstead et al., GEO: GSE72249; Glont et al., GEO: GSE112969; Kong et al., GEO: GSE26831, GEO: GSE23893; Franco et al., GEO: GSE59530; Liu et al., GEO: GSE60272; Hurtado et al., GEO: GSE25710; Toropainen et al., GEO: GSE56086; Malinen et al., GEO: GSE83860; Pihlajamaa et al., GEO: GSE47192. More details are provided in Table S1.

Cell Reports, Volume *28*

Supplemental Information

Meta-analysis of Chromatin Programming by Steroid Receptors

Ville Paakinaho, Erin E. Swinstead, Diego M. Presman, Lars Grøntved, and Gordon L. Hager

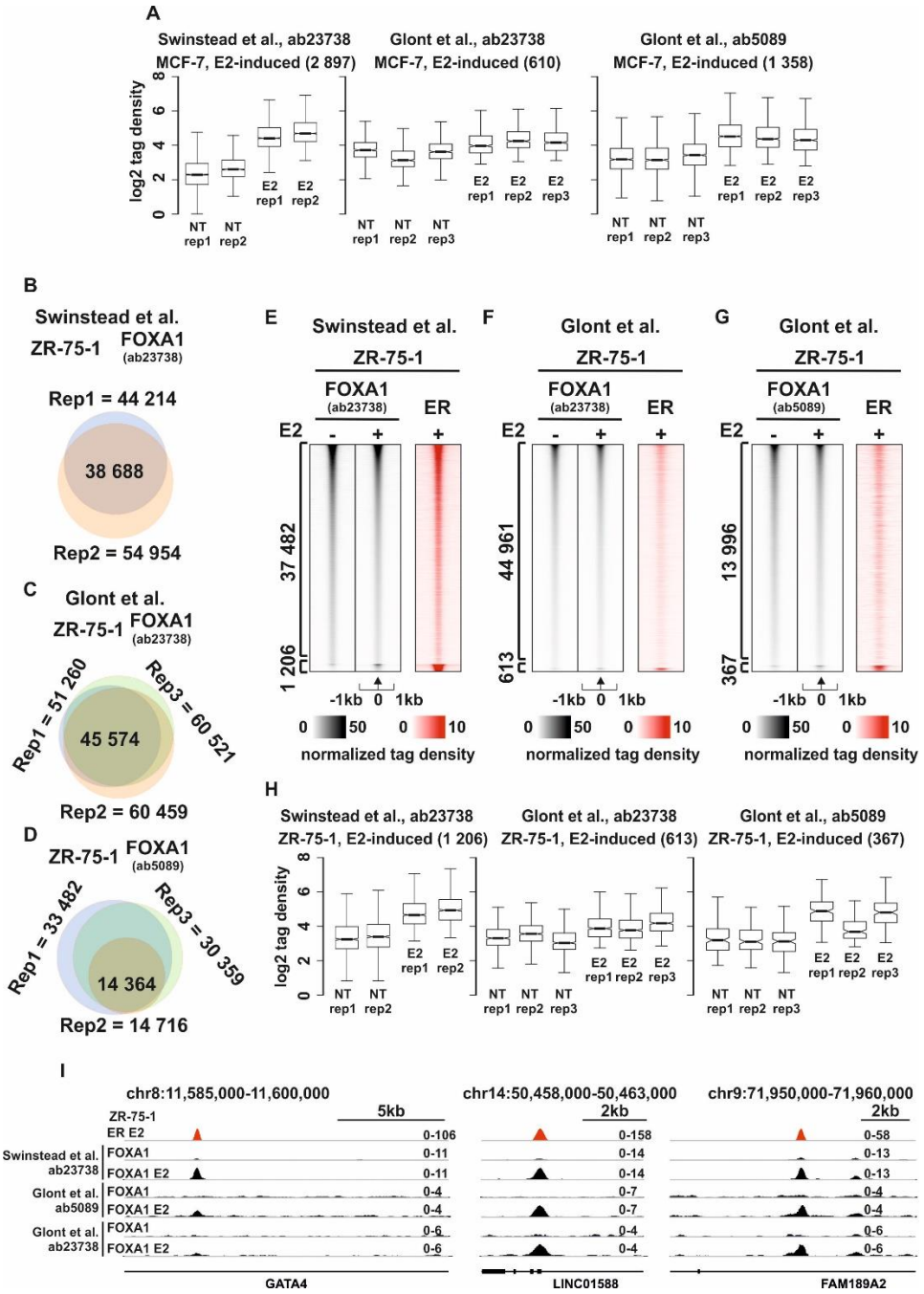

Figure S1. E2-induced binding of FOXA1 in ZR-75-1 cells. Related to Figure 1. (A) Normalized log2 tag density of E2-induced FOXA1 binding sites from MCF-7 cells. Data are shown for each biological replicate sample. Log2 tag density depicted as box plots and normalized to a total of 10 million reads. NT, vehicle or non-treated sample. (B-D) Comparison of identified FOXA1+E2 peaks from biological replicate samples using data sets from Swinstead et al. (B) and Glont et al. (C-D). Number of peaks identified in each replicate and the concordant peaks are shown. Used FOXA1 antibody is depicted in the parenthesis. (E-G) Heat maps represent FOXA1 (black) and ER (red) ChIP-seq, with unchanged sites on top of the heat map, and E2-induced FOXA1 sites on the bottom of the heat map. The number of binding sites is shown on the left of the heat map. Each heat map represents ±1kb around the center of the FOXA1 peak. Binding intensity scale is noted below on a linear scale. Heat maps are sorted based in FOXA1+E2 binding intensity. All heat maps are normalized to a total of 10 million reads, and to tags per bp per site. Used FOXA1 antibody is depicted in the parenthesis. (H) Normalized log2 tag density of E2-induced FOXA1 binding sites from ZR-75-1 cells. Data are presented as in (A). (I) Three representative genome browser track examples of E2-induced FOXA1 binding sites. Genome browser tracks are normalized to a total of 10 million reads.

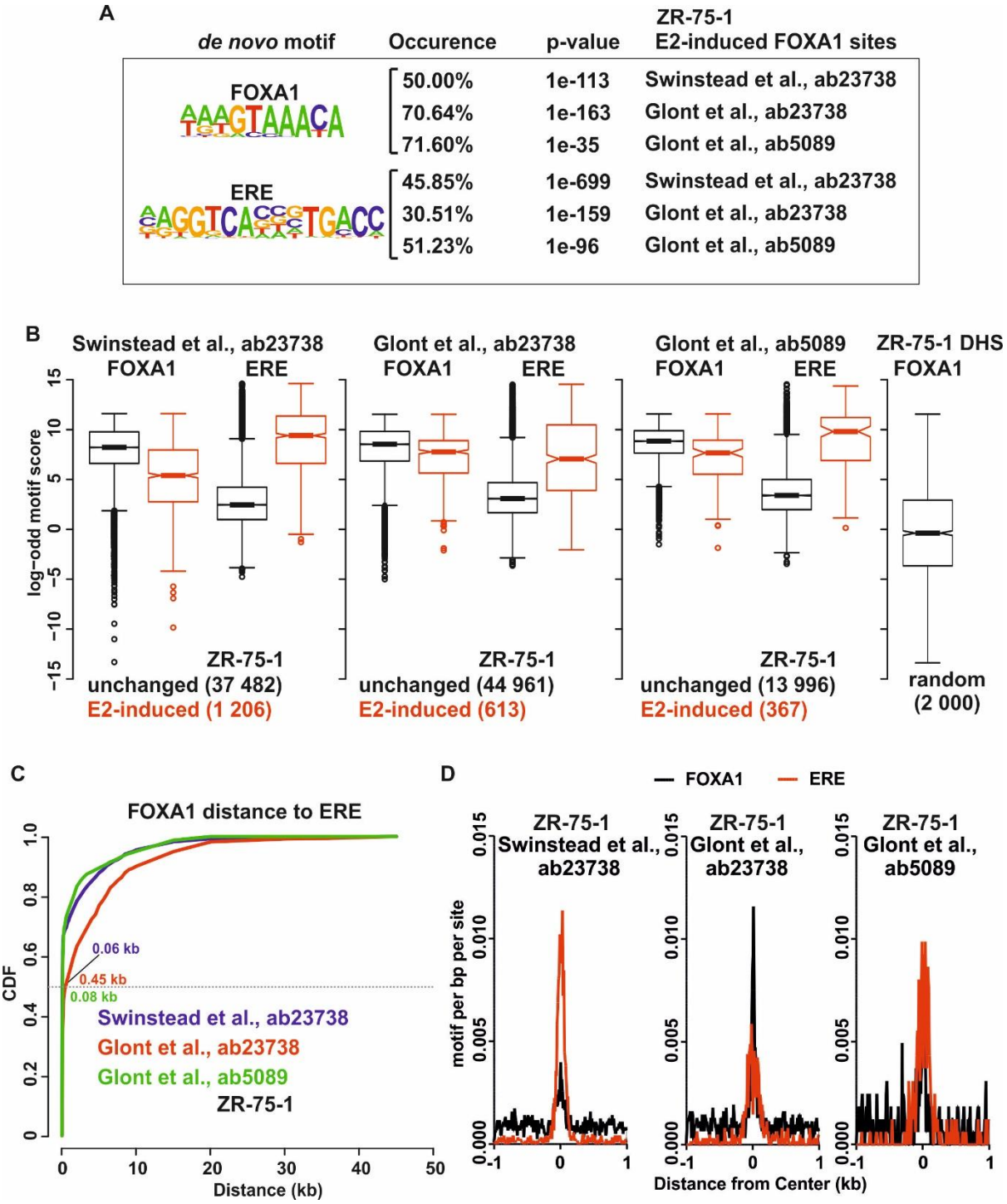

Figure S2. ERE and forkhead motif are both enriched at E2-induced FOXA1 sites in ZR-75-1 cells. Related to Figure 2. (A) *De novo* motif analysis of ERE and FOXA1 motif enrichment at E2-induced FOXA1 sites from indicated data sets. Percentage of occurrence, and motif enrichment p-value is shown. (B) Log-odd motif scores of FOXA1 or ERE at unchanged (black) or E2-induced (red) FOXA1 sites from indicated data sets. Also displayed is FOXA1 motif scores from random DHS in ZR-75-1 cells. Motif score distribution depicted as box plots. (C) Cumulative distribution function (CDF) of distance between E2-induced FOXA1 site and closest ERE in indicated data sets. Median is depicted by grey dashed line, and median from each data set is indicated with color coding. (D) Aggregate plot of FOXA1 motif (black) and ERE (red) enrichment at E2-induced FOXA1 sites from indicated data sets. Plots are normalized to a total of 10 million reads, and to motif per bp per site.

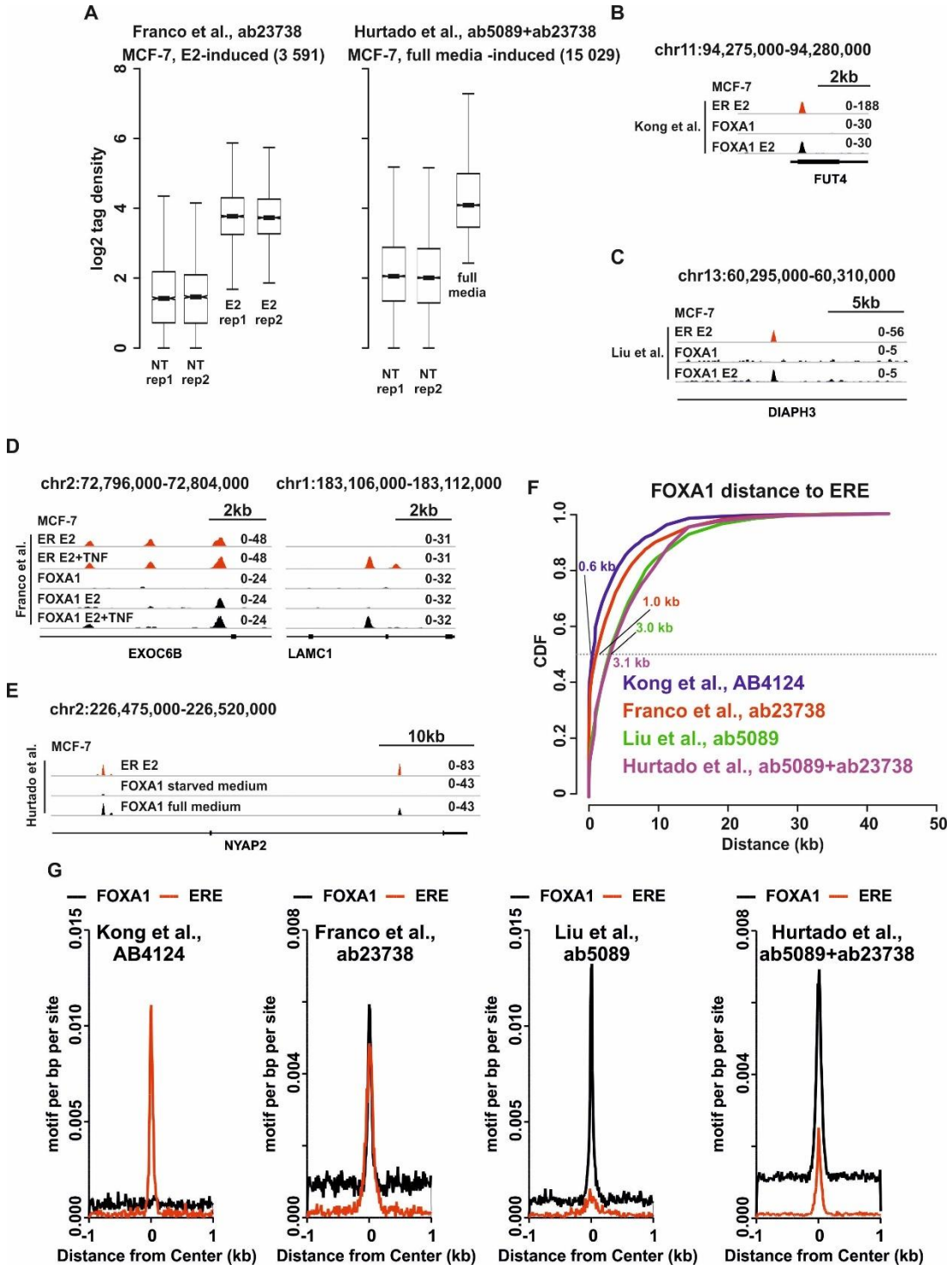

Figure S3. ERE and forkhead motif are both enriched at E2-induced FOXA1 sites in MCF-7 data from several investigators. Related to Figure 3. (A) Normalized log2 tag density of E2/full media-induced FOXA1 binding sites from Franco et al. and Hurtado et al. data sets. Data are shown for each biological replicate sample. Log2 tag density depicted as box plots and normalized to a total of 10 million reads. NT, vehicle or non-treated sample. (B-E) Representative genome browser track examples of E2/full media -induced FOXA1 binding sites for Kong et al. (B), Liu et al. (C), Franco et al. (D), and Hurtado et al. (E) data sets. Genome browser tracks are normalized to a total of 10 million reads. (F) Cumulative distribution function (CDF) of distance between E2-induced FOXA1 site and closest ERE in indicated data sets. Median is depicted by grey dashed line, and median from each data set is indicated with color coding. (G) Aggregate plot of FOXA1 motif (black) and ERE (red) enrichment at E2/full media-induced FOXA1 sites from indicated data sets. Plots are normalized to a total of 10 million reads, and to motif per bp per site.

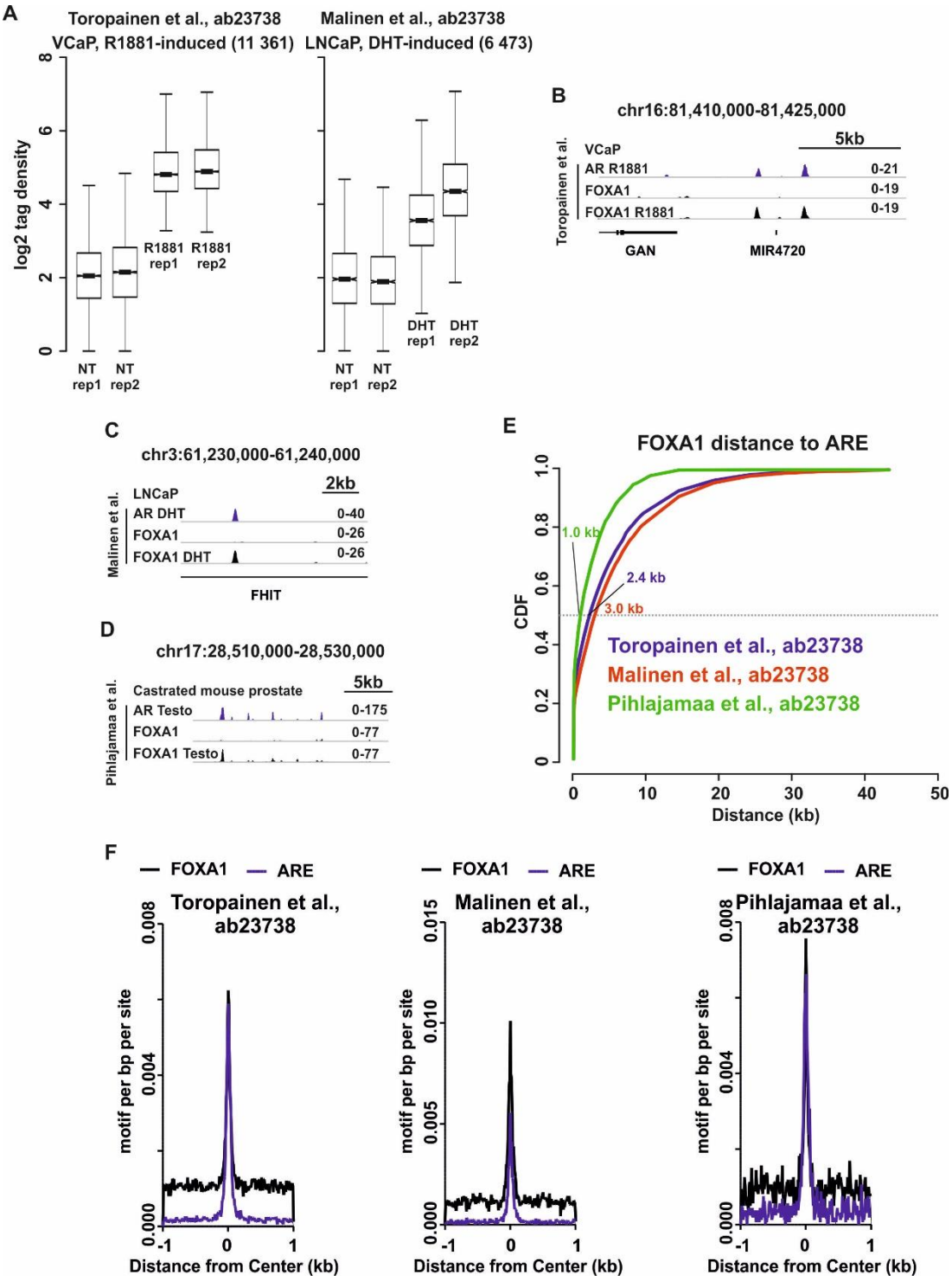

Figure S4. ARE and forkhead motif are both enriched at androgen-induced FOXA1 sites. Related to Figure 4. (A) Normalized log2 tag density of androgen-induced FOXA1 binding sites from Toropainen et al. and Malinen et al. data sets. Data are shown for each biological replicate sample. Log2 tag density depicted as box plots and normalized to a total of 10 million reads. NT, vehicle or non-treated sample. (B-D) Representative genome browser track examples of androgen-induced FOXA1 binding sites for Toropainen et al. (B), Malinen et al. (C), and Pihlajamaa et al. (D) data sets. Genome browser tracks are normalized to a total of 10 million reads. (E) Cumulative distribution function (CDF) of distance between androgen-induced FOXA1 site and closest ARE in indicated data sets. Median is depicted by grey dashed line, and median from each data set is indicated with color coding. (F) Aggregate plot of FOXA1 motif (black) and ARE (blue) enrichment at androgen-induced FOXA1 sites from indicated data sets. Plots are normalized to a total of 10 million reads, and to motif per bp per site.

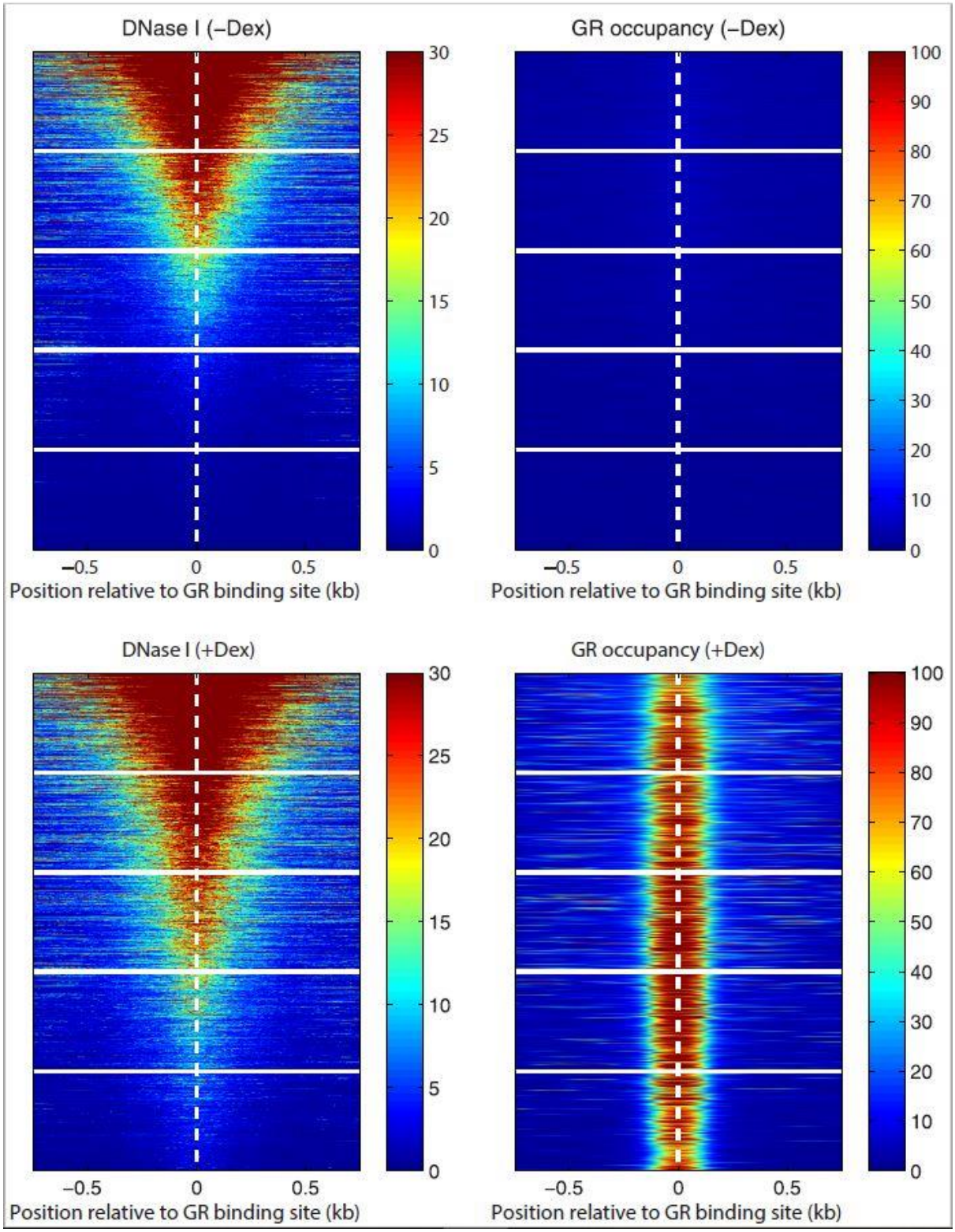

Figure S5. GR enhancers can be hypersensitive or insensitive to DNase I. Related to Figure 5. Heat maps of DNase I accessibility (cut count density) and GR occupancy at all GR-enhancers in 3134 cells (Johnson et al., 2018). GR enhancers were sorted by the average level of DNase I sensitivity before hormone treatment (highest at the top). The heat map scale is linear; red: high occupancy; blue: low occupancy.